Crater production by energetic nanoparticle impact on Au nanofoams

Christian Anders, Eduardo M. Bringa, and Herbert M. Urbassek'

Citation: Appl. Phys. Lett. **108**, 113108 (2016); doi: 10.1063/1.4944420
View online: http://dx.doi.org/10.1063/1.4944420
View Table of Contents: http://aip.scitation.org/toc/apl/108/11
Published by the American Institute of Physics

Crater production by energetic nanoparticle impact on Au nanofoams

Christian Anders,[1] Eduardo M. Bringa,[2] and Herbert M. Urbassek[1,a)]
[1]*Physics Department and Research Center OPTIMAS, University Kaiserslautern, Erwin-Schrödinger-Straße, D-67663 Kaiserslautern, Germany*
[2]*CONICET and Facultad de Ciencias Exactas y Naturales, Universidad Nacional de Cuyo, Mendoza 5500, Argentina*

(Received 19 November 2015; accepted 5 March 2016; published online 16 March 2016)

Impact of energetic nanoparticles on solids produces craters on the surface. We use molecular dynamics simulations to compare crater production on a compact Au solid with that in a porous (foam) target. Our results show a complex picture: (i) At low impact velocities, the nanoparticles produce permanent craters in the foam while they cannot penetrate the compact target. (ii) With increasing velocity and/or projectile mass, the crater depth in the foam target increases less strongly than for the compact target. The plasticity-affected zone in the foam target is of similar size as in the compact target. Our results are relevant for the use of porous structures as shields against nanoparticle impact. © *2016 AIP Publishing LLC*. [http://dx.doi.org/10.1063/1.4944420]

Nanoparticle (NP) impact on solids may lead to permanent damage on the solid surface. While at small impact velocities, NPs are deposited on the surface, they produce large craters at higher velocity.[1] Such processes are relevant in dusty plasmas[2] and in the space environment where dust grains—but also metallic debris—may damage the surfaces of spacecraft;[3–7] they are also employed beneficially for the removal of material for surface-analytic purposes.[8,9] Thibeault *et al.*[10] summarized the recent research activities on using nanomaterials for radiation protection in space.

Recently, the availability of metallic foams spurred activity to investigate the radiation resistance of these materials.[11–15] Indeed, it was found that the high surface-to-volume ratio increases the annealing of radiation-induced defects. While these studies focused on the impact of single ions on foam structures, the response of foam materials to NP bombardment is also relevant. The use of light-weight foam materials may be particularly useful as shields against NP impact in space environment. A macroscopic argument requires the same amount of target mass (column) as in a compact target to stop the projectile. Then the crater depths d_{foam} in the foam and d_{bulk} in the compact target scale as the inverse target density

$$\frac{d_{\mathrm{foam}}}{d_{\mathrm{bulk}}} = \frac{n_{\mathrm{bulk}}}{n_{\mathrm{foam}}} = \frac{1}{\phi}\,, \tag{1}$$

where $\phi = n_{\mathrm{foam}}/n_{\mathrm{bulk}}$ denotes the foam filling factor. Foams are useful shields against NP impact if they require less mass than a compact target and thus $d_{\mathrm{foam}}/d_{\mathrm{bulk}} < 1/\phi$.

Molecular dynamics (MD) simulations have been used to study in detail the characteristics of crater formation in compact solids under NP impact.[16–19] Let us denote by N the number of atoms in the projectile NP, v its velocity, and $E = mv^2/2$ the impact energy per atom; m is the atomic mass. It was found that a threshold energy E_{th} is needed to induce cratering in the surface; soon after the onset of cratering, craters assume a hemispheric form. Above this threshold, the crater volume increases linearly with energy

$$V = a(E - E_{\mathrm{th}}), \tag{2}$$

and hence the crater depth follows:

$$d = b(E - E_{\mathrm{th}})^{1/3}. \tag{3}$$

In the present paper, we use MD simulations to compare NP impact on compact solids with foam structures. The simulations have been performed using the molecular dynamics simulation software LAMMPS.[20] Besides a single-crystalline Au target, a Au foam target is used; the latter has been constructed from a prototype generated as in Refs. 21 and 22. The foam structure has a filling factor of $\phi = 0.55$ and the average size of the grains ("filaments") amounts to $D = 3$ nm. The targets have dimensions of 734×734 Å^2 in lateral direction and 550 Å in depth, containing 9.36×10^6 atoms. Both the foam and the compact target have a (100) free surface. Before the start of the impact simulations, the targets are relaxed to 0 K. At the lateral and bottom sides, damped boundary conditions are used which mimic energy dissipation to the surrounding target material.

The targets are bombarded by spherical Au NPs with radius R, containing N atoms. We study projectiles with sizes between $N = 10^4$ and 2×10^5 atoms and impact velocities v between 0.5 and 10 km/s. Our minimum NP size of $N = 10^4$ has been chosen such that its radius $R = 3.5$ nm is larger than the filament radius, $R > D$. Thus in all cases the dependence of the impact event on the exact impact position can be neglected.[17] Note that cluster impacts on compact targets show negligible fluctuations already for cluster sizes as small as $N = 12$.[23,24] Hence, for each velocity only one impact has been simulated for foam and compact target, respectively. We follow the simulations up to a time of 241 and 321 ps after an impact on the foam and compact targets, respectively, until the crater form has stabilized.

The interaction between the Au atoms is modeled by a many-body potential, which reproduces the melting temperature of Au, $T_m = 1338$ K.[24–26] At these low impact energies,

a)Electronic mail: urbassek@rhrk.uni-kl.de. URL: http://www.physik.uni-kl.de/urbassek/

the influence of electronic stopping is only minor; therefore, no electronic stopping has been applied.

In Fig. 1, we compare the results of NP impact on a compact and a foam target for the exemplary case of 5 km/s impact of a Au_{10000} NP. Data of the pressure and density have been evaluated in a cylinder of radius 2 nm—smaller than the NP, but sufficiently large for local averaging—on the axis immediately below the NP impact point.

Due to the impact, the hydrostatic pressure increases strongly below the NP and reaches the value of almost 170 GPa in the compact target; the values are smaller in the foam structure, where only 100 GPa are reached. In both systems, a compressive pressure wave then runs into the target interior. Its velocity is smaller in the foam (3.3 km/s) than in the compact material (4.8 km/s); for comparison, the longitudinal velocity of sound in Au in [100] direction is 2.5 km/s. The sound speed in foams is known to be smaller than that in the compact targets.[27] However, the wave front is sharper in the compact target than in the foam, since the inhomogeneous structure of the foam blurs the wave front. The wave amplitude diminishes with time since the impact energy is radiated three-dimensionally into the target interior. Note that after the compression stage, the pressure turns tensile close to the surface at times of around 2 ps; this corresponds to the crater excavation stage. We conclude that similar to compact targets, NP impact generates a shock wave in the foam.

The density profiles show that close to the surface the crater is excavated; in contrast, the material in the compressive pressure pulse is compacted. Interestingly, both the compaction and the crater excavation in the foam follow closely that of the compact target.

Fig. 2 displays the final state of the irradiated targets at the end of the simulation at the same scale. Here an impact velocity of 10 km/s was chosen to emphasize crater and defect formation. Defects have been characterized using the Ackland-Jones detector.[28] We first note that the crater has cooled better when surrounded by the compact material; only small melt nests in the crater rim have survived, which are displayed as "disordered atoms" in Fig. 2. In the foam target, in contrast, the entire crater walls are covered by a melt pool; this is caused by both the higher temperatures reached in the foam target and the poorer heat conduction in the foam filaments. The crater wall in the foam has become compact as the filaments have been crushed, see Fig. 2(b).

Defects extend deeply into the material; these are visible in Fig. 2 mainly as stacking-fault planes which indicate the formation of dislocations and plasticity by the impact. Note that some stacking fault planes existed in the foam target already at the foam production stage (see filaments at bottom of figure). The plastic zone has a width of 136 Å in the compact target and is hence larger than the crater depth (108 Å) itself. In contrast, for the foam target the crater reaches a depth of 327 Å, while the width of the plastic zone amounts to 133 Å. Thus, the plastic zones are of similar width in the two targets since the newly generated defects are mainly found in the compactified region.

Fig. 3(a) shows how crater sizes depend on the impact velocity of the Au_{10000} NPs. For the compact target, small impact velocities (below approximately 2 km/s) do not lead to a crater; the NP is rather deposited on the surface. The foam, however, is more easily crushed and even small velocities are able to form a crater. The reason is that in a compact target, the crater volume has to be excavated by pushing the material onto the surface; for a foam it is easier to deform the filaments and push the excavated crater material into the interior.

We also display the plastic-zone depths in Fig. 3(a); these are considerably larger than the crater depths themselves, indicating the important role played by dislocation damage.

For the foams the determination of the depth of the plastic zone is not trivial, since already before bombardment, the

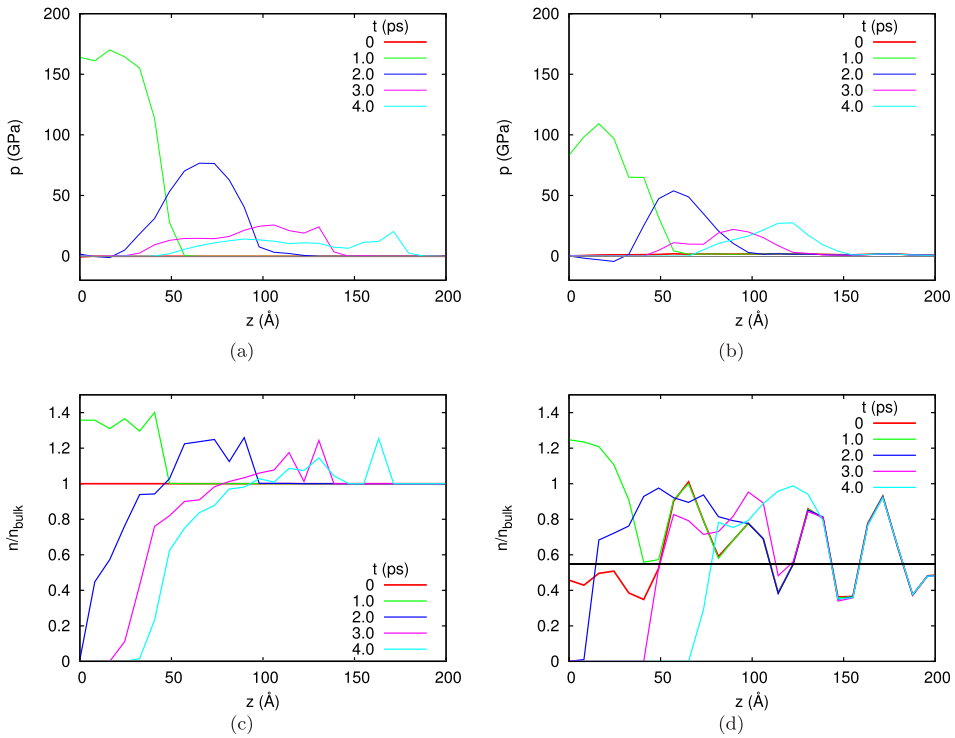

FIG. 1. Depth profiles of pressure, p, and density, n, on the axis below the Au_{10000} NP impacting with 5 km/s for the compact (left) and foam (right) target at the times indicated. The density has been normalized to the density of the compact target, n_{bulk}; the average density of the foam target is indicated by a black line in subfigure (d).

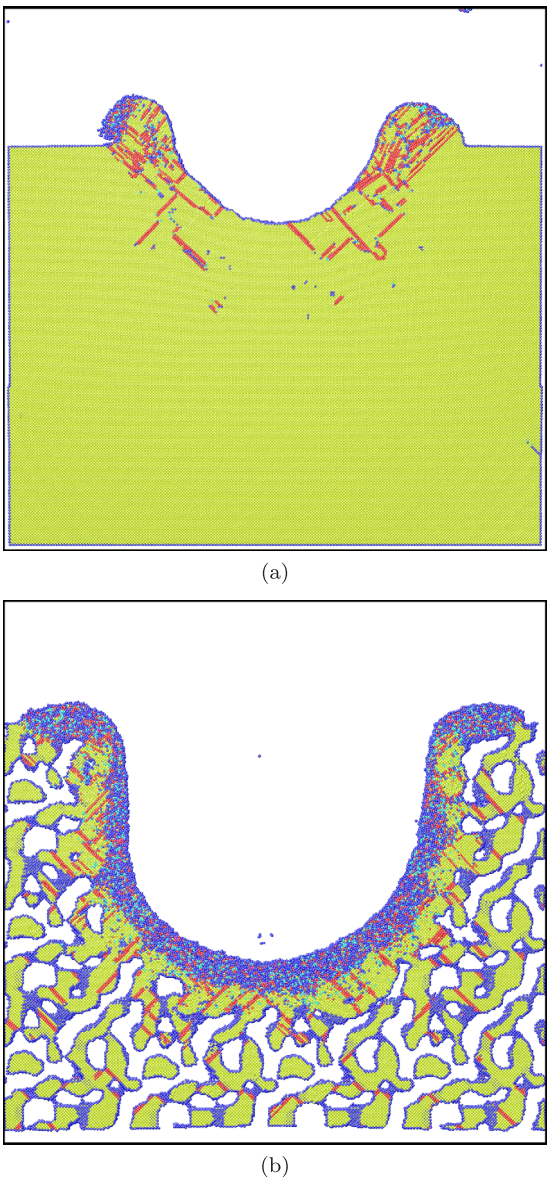

FIG. 2. Final state of the (a) compact and the (b) foam target after impact of a 10 km/s Au_{10000} NP. Both snapshots show a cross-sectional view (thickness 6 Å, width 75 nm) at the same scale at the end of the simulation. Color codes the local crystal structure as determined by the Ackland-Jones detector:[28] fcc (yellow), hcp (red), disordered (blue), and bcc (cyan).

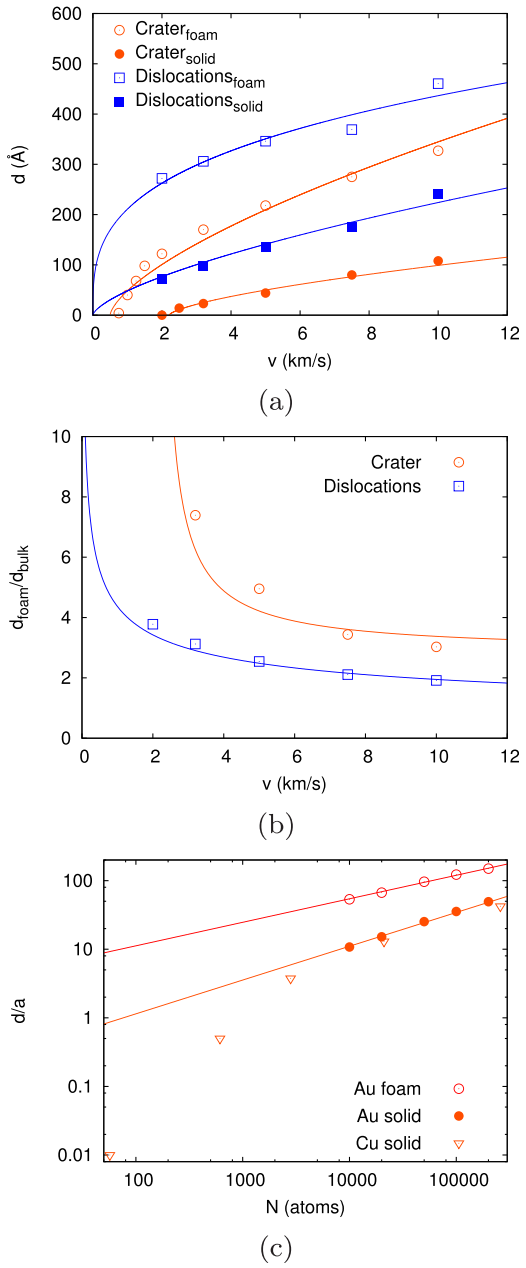

FIG. 3. (a) Crater depth (circles) and plastic-zone depth (squares) vs impact velocity for Au NP impact on a Au compact and a Au foam target. Lines give fits to Eq. (3). (b) Enhancement of depth in a foam target over that in a compact target. (c) Dependence of the crater depth on the size N of NPs for an impact velocity of 5 km/s. Additional data for Cu NPs impinging with a velocity of 5.5 km/s on a Cu compact target taken from Ref. 17 by scaling the crater depth d to the lattice constant a. Lines show power-law scaling.

filaments are not defect-free. For the smallest impact velocities, we therefore do not indicate the plastic-zone depths. While the plastic-zone width in the foams is around 135 Å for all impact velocities, it increases slightly in the compact target from 80 Å at $v = 2$ km/s to around 135 Å at $v = 10$ km/s.

The crater depth d follows a power law with impact energy, Eq. (3), with parameters $b = 20.7$ (72.3) Å/(eV/atom)$^{1/3}$ and the threshold energy $E_{\mathrm{th}} = 8.2$ (0.58) eV/atom for the compact (foam) target. For the foam target, the threshold velocity is considerably smaller than for the compact target; this is due to the high deformability of the foam target. For dislocation production—in either target—no threshold is apparent and the data can be fitted with $E_{\mathrm{th}} = 0$, Eq. (3). This is plausible since cluster impact may produce damage inside the target even without creating a crater.

Fig. 3(b) directly compares the crater sizes of foam and compact targets by displaying the ratio $d_{\mathrm{foam}}/d_{\mathrm{bulk}}$. The simple estimate of Eq. (1) would assume that the crater size scales with the inverse foam density, and hence $d_{\mathrm{foam}}/d_{\mathrm{bulk}} = 1/\phi \cong 1.8$ in our case. We observe that in the velocity range investigated here, the crater depth in foam targets is considerably larger than predicted. This is caused by the threshold behavior of crater formation in bulk targets, Eq. (3), since the threshold in foams is much smaller than in compact targets. Indeed, with increasing velocity the ratio $d_{\mathrm{foam}}/d_{\mathrm{bulk}}$ decreases and appears to converge to the prediction, $d_{\mathrm{foam}}/d_{\mathrm{bulk}} \cong 1.8$.

Fig. 3(c) finally shows how crater depths change with the size N of the impinging NPs. They follow a power law,

$d \propto N^{\alpha}$, with $\alpha = 0.49$ (0.34) for the compact (foam) target. Plastic-zone depths (not shown) increase with the same exponents. We note that previous data of Cu NPs impinging on a Cu compact target[17] follow (for large N) exactly the same law as the Au data. The Cu data for smaller NP sizes show a strong decrease for smaller clusters, $N \lesssim 10^4$, which has been interpreted as a threshold behavior.[17]

We conclude that crater depths increase more strongly with projectile size in the compact target than in the foam target. Hence, the ratio $d_{\mathrm{foam}}/d_{\mathrm{bulk}}$ decreases with increasing N and approaches the prediction of Eq. (1), $d_{\mathrm{foam}}/d_{\mathrm{bulk}} = 1/\phi$. This decrease is caused by the fact that for increasingly large NPs, the foam appears just as a homogeneous bulk target with reduced density.

In summary, we use molecular dynamics simulations to compare crater production by NP impact on a compact Au solid with that in a porous (foam) target. We find that the threshold for crater formation is considerably reduced in foam targets, since the filament structures are easily deformed. Crater walls consist of compactified foam material, containing a large amount of defects (stacking faults and dislocations). The thickness of the plastic zone is of similar size as in compact targets. Compactification of the crater walls is accompanied by considerable heating leading to extensive melting. A macroscopic argument predicts that the crater depth scales as the inverse foam density, Eq. (1). However, due to the different thresholds for compact and foam targets, craters formed at low velocities in foams are actually larger than according to the macroscopic prediction. For higher impact velocities and for larger NPs, crater depths tend to comply with Eq. (1). We conclude that at small velocities, and for small projectiles, the foam offers no advantage over compact solids in shielding against NP impacts.

We thank Diana Farkas for providing the porous sample. EMB would like to thank funding from PICT2009-0092 and a SeCTyP grant. Simulations were performed at the High Performance Cluster Elwetritsch (RHRK, TU Kaiserslautern, Germany).

[1]H. Hsieh, R. S. Averback, H. Sellers, and C. P. Flynn, Phys. Rev. B **45**, 4417 (1992).
[2]A. Bouchoule, Phys. World **6**(8), 47 (1993).
[3]R. E. Johnson, *Energetic Charged-Particle Interactions with Atmospheres and Surfaces* (Springer, Berlin, 1990).
[4]G. A. Graham, N. McBride, A. T. Kearsley, G. Drolshagen, S. F. Green, J. A. M. McDonnell, M. M. Grady, and I. P. Wright, Int. J. Impact Eng. **26**, 263 (2001).
[5]S. Jurac, M. A. McGrath, R. E. Johnson, J. D. Richardson, V. M. Vasyliunas, and A. Eviatar, Geophys. Res. Lett. **29**, 2172, doi:10.1029/2002GL015855 (2002).
[6]L. S. Novikov, V. N. Mileev, E. N. Voronina, L. I. Galanina, A. A. Makletsov, and V. V. Sinolits, J. Surf. Investigation **3**, 199 (2009).
[7]E. Grossman, I. Gouzman, and R. Verker, MRS Bull. **35**, 41 (2010).
[8]N. Winograd, Anal. Chem. **77**, 142A (2005).
[9]N. Winograd and B. J. Garrison, Annu. Rev. Phys. Chem. **61**, 305 (2010).
[10]S. A. Thibeault, J. H. Kang, G. Sauti, C. Park, C. C. Fay, and G. C. King, MRS Bull. **40**, 836 (2015).
[11]J. F. Rodriguez-Nieva, E. M. Bringa, T. A. Cassidy, R. E. Johnson, A. Caro, M. Fama, M. J. Loeffler, R. A. Baragiola, and D. Farkas, Astrophys. J. Lett. **743**, L5 (2011).
[12]E. M. Bringa, J. D. Monk, A. Caro, A. Misra, L. Zepeda-Ruiz, M. Duchaineau, F. Abraham, M. Nastasi, S. T. Picraux, Y. Q. Wang *et al.*, Nano Lett. **12**, 3351 (2012).
[13]E. G. Fu, M. Caro, L. A. Zepeda-Ruiz, Y. Wang, K. Baldwin, E. Bringa, M. Nastasi, and A. Caro, Appl. Phys. Lett. **101**, 191607 (2012).
[14]J. F. Rodriguez-Nieva and E. M. Bringa, Nucl. Instrum. Methods Phys. Res., Sect. B **304**, 23 (2013).
[15]C. Anders, E. M. Bringa, and H. M. Urbassek, Nucl. Instrum. Methods Phys. Res., Sect. B **342**, 234 (2015).
[16]J. Samela and K. Nordlund, Phys. Rev. Lett. **101**, 027601 (2008).
[17]C. Anders, E. M. Bringa, F. D. Fioretti, G. Ziegenhain, and H. M. Urbassek, Phys. Rev. B **85**, 235440 (2012).
[18]C. Anders, G. Ziegenhain, C. J. Ruestes, E. M. Bringa, and H. M. Urbassek, New J. Phys. **14**, 083016 (2012).
[19]C. Anders, E. M. Bringa, G. Ziegenhain, G. A. Graham, J. F. Hansen, N. Park, N. E. Teslich, and H. M. Urbassek, Phys. Rev. Lett. **108**, 027601 (2012).
[20]S. Plimpton, J. Comput. Phys. **117**, 1 (1995); see http://lammps.sandia.gov/.
[21]D. A. Crowson, D. Farkas, and S. G. Corcoran, Scr. Mater. **56**, 919 (2007).
[22]D. A. Crowson, D. Farkas, and S. G. Corcoran, Scr. Mater. **61**, 497 (2009).
[23]T. J. Colla, R. Aderjan, R. Kissel, and H. M. Urbassek, Phys. Rev. B **62**, 8487 (2000).
[24]S. Zimmermann and H. M. Urbassek, Nucl. Instrum. Methods Phys. Res., Sect. B **255**, 208 (2007).
[25]T. J. Colla and H. M. Urbassek, Nucl. Instrum. Methods Phys. Res., Sect. B **164–165**, 687 (2000).
[26]S. Zimmermann and H. M. Urbassek, Nucl. Instrum. Methods Phys. Res., Sect. B **228**, 75 (2005).
[27]N. Ramakrishnan, Bull. Mater. Sci. **17**, 499 (1994).
[28]G. J. Ackland and A. P. Jones, Phys. Rev. B **73**, 054104 (2006).